Eur. Phys. J. C (2022) 82:294
https://doi.org/10.1140/epjc/s10052-022-10257-5

THE EUROPEAN PHYSICAL JOURNAL C

Regular Article - Theoretical Physics

Gravitational collapse involving electric charge in the decoupling limit of the dilatonic Gauss–Bonnet gravity

Anna Nakonieczna[a], **Łukasz Nakonieczny**[b]

Faculty of Physics, Institute of Theoretical Physics, University of Warsaw, Pasteura 5, 02-093 Warsaw, Poland

Received: 18 September 2021 / Accepted: 26 March 2022 / Published online: 4 April 2022

Abstract The paper discusses gravitational collapse of an electrically charged scalar field in the decoupling limit of the dilatonic Gauss–Bonnet gravity. The emerging spacetimes contained Schwarzschild black holes for sufficiently big scalar fields self-interaction strengths. Dependencies of the collapse characteristics on the dilatonic and Gauss–Bonnet parameters turned out to be similar in the case of black hole masses and radii as well as their time of formation in terms of retarded time. In the cases of masses and radii minima were observed, while in the remaining case a maximum existed. The electric charge of the emerging black holes possessed a maximum when measured versus the dilatonic coupling constant and was strictly decreasing with the Gauss–Bonnet coupling. The times of formation and charges of black holes decreased, while masses and radii increased with the self-interaction strengths of the dynamical fields. Values of the energy density, radial pressure, pressure anisotropy and the collapsing scalar fields were the biggest along the hypersurface of propagation of the scalar fields initial peaks. For big values of the Gauss–Bonnet coupling constant, an increase in their values was also observed in the vicinity of the central singularity within the whole range of advanced time. Non-zero values of the dilaton field outside the black hole event horizon may indicate a formation of a hairy black hole. The local temperature calculated along the apparent horizon was increasing for late times of the evolution and exhibited extrema in areas, where the dynamics of the gravity–matter system was observed.

Contents

[a] e-mail: Anna.Nakonieczna@fuw.edu.pl (corresponding author)
[b] e-mail: Lukasz.Nakonieczny@fuw.edu.pl

1 Introduction

Dynamical gravitational collapse is a fully non-linearly and non-perturbatively described process in which a mutual evolution of the spacetime geometry and matter content of the evolving spacetime is tracked. It means that these two features affect each other in the course of the process and hence the described outcomes are closer to reality, but at the same time more difficult to obtain than in the case of matter evolutions on predefined backgrounds, even if backreaction is considered. When an electrically charged scalar field is included in the examined matter–geometry system, the whole system can be regarded as simulating real astrophysical evolutions. Thus obtained spacetime structures satisfactorily resemble the structures anticipated in the case of a non-charged, but rotating collapse, which takes place during real astrophysical events [1,2].

Up to now, structures of spacetimes emerging from the dynamical gravitational collapse were extensively studied first in the simplest cases of sole self-interacting neutral [3] and electrically charged [4–8] scalar fields. More sophisticated theories, complicated in either or both gravitational and matter sectors were studied in [9–20]. Apart from investigating structures of spacetimes forming in the process of interest, additional problems related to gravitational dynamics, such as pair creation during collapse and subsequent

evaporation of black holes, issues of the cosmic censorship conjecture and the information loss problem, the impact of changing the number of dimensions and the role of various topologies, time measurements as well as observables, were discussed in [1,2,7–9,11,21–27]. The up-to-date summary of the sketched researches can be found in [28].

The Einstein–dilaton–Gauss–Bonnet (EdGB) theory is a beyond general relativity formulation, which is a scalar–tensor theory including higher order terms in curvature. It has been extensively studied in various cosmological large-scale contexts such as dark energy explanations, inflation, early universe bouncing models or cosmological perturbations [29–31]. It has been also involved in small-scale astrophysical analyses like investigating black holes and their mergers or creation and stability of wormholes [32–35]. Experimental predictions of the EdGB theory are consistent with current general relativity tests, but the theory yields different results for mergers of the stellar mass black holes [36], what makes it interesting in the context of analyses of the recently extremely viable gravitational waves observations.

So far, a spherical gravitational collapse in the EdGB theory was considered within its shift symmetric version in [37]. The research was conducted in coordinates which do not penetrate the horizon, hence the collapse results were described up to the forming horizon and its interior was not analysed. This successful attempt to describe the outcomes of a fully non-linear process within the EdGB theory was an introductory step towards analysis of the whole spacetime, including interiors of emerging singular objects. Our current studies present another approach to this problem, namely the engaged coordinates cover the whole spacetime, yet their usage also requires introducing a simplification of the full EdGB theory.

The decoupling limit of the EdGB theory is a version of the full theory, in which the Gauss–Bonnet term is not included in the derivation of the Einstein equations, only in the equations describing the matter sector of the theory. This means that the scalar sector of the theory does not backreact on geometry [34]. This simplified formulation of the full EdGB theory has been recently employed in research on black hole hair formation and scalar modes [38–40]. Investigating the collapse within the truncated version of the EdGB theory will be performed in double null coordinates, which enable to trace the gravitational evolution within the whole spacetime, that is from approximately null infinity up to the central singularity. This is the first step towards investigations of the course and results of gravitational evolutions in the full version of the EdGB theory in the whole forming spacetimes, not only regions exterior to the nascent singular objects.

The paper is organized as follows. In Sect. 2 the considered model was presented. Section 3 contains details of numerical calculations and results analysis. The obtained results were described and discussed in Sects. 4–6. Section 7 summarizes the undertaken research. Technical details of the numerical code preparation and its tests are presented in Appendix A.

2 Theoretical model of the evolution

The studied theoretical model of the dynamical collapse involves an electrically charged scalar field collapsing within the decoupling limit of the dilaton–Gauss–Bonnet gravity. The general form of the action written, due to the fact that the whole construction involves the string theory concepts, in the string frame is the following:

$$\hat{S} = \int d^4x\sqrt{-\hat{g}} \times \left\{ e^{-2\phi}\left[\hat{R} - 2\left(\hat{\nabla}\phi\right)^2 + e^{2\alpha\phi}\left(\hat{\mathcal{L}}_{SF} + \gamma\hat{\mathcal{L}}_{GB}\right)\right]\right\}, \tag{2.1}$$

where ϕ stands for the dilaton field, α is the dilatonic coupling constant and γ determines the coupling between the Gauss–Bonnet contribution and the dilaton. The geometrized units system, in which $8\pi G = c = 1$, was used in the computations. The Lagrangian of the electrically charged scalar field ψ is given by the expression

$$\hat{\mathcal{L}}_{SF} = -\frac{1}{2}\hat{D}_\beta\psi\left(\hat{D}^\beta\psi\right)^* - F_{\beta\sigma}F^{\beta\sigma}, \tag{2.2}$$

where $F_{\beta\sigma}$ is the Maxwell field strength tensor. The covariant derivative is $\hat{D}_\beta = \hat{\nabla}_\beta + ieA_\beta$, where e is the electric coupling constant, A_β is the four-potential and i denotes the imaginary unit. The Gauss–Bonnet Lagrangian is defined in a standard way

$$\hat{\mathcal{L}}_{GB} = \hat{R}^2 - 4\hat{R}_{\beta\sigma}\hat{R}^{\beta\sigma} + \hat{R}_{\beta\sigma\gamma\delta}\hat{R}^{\beta\sigma\gamma\delta}. \tag{2.3}$$

The variation of the constructed action (2.1) with respect to matter fields, namely the dilaton field ϕ, the Maxwell field A_μ and the complex scalar field ψ results in the following set of evolution equations:

$$\nabla^2\phi - \frac{\alpha+1}{4}e^{2\phi(\alpha+1)}D_\nu\psi\left(D^\nu\psi\right)^* - \frac{1}{2}\alpha e^{2\alpha\phi}F_{\beta\sigma}F^{\beta\sigma} + 2\gamma\alpha e^{2\alpha\phi}\hat{\mathcal{L}}_{GB} = 0, \tag{2.4}$$

$$\nabla_\mu\left(e^{2\alpha\phi}F^{\mu\nu}\right) + \frac{1}{4}e^{2\phi(\alpha+1)}\left[ie\psi^*D^\nu\psi - ie\psi\left(D^\nu\psi\right)^*\right] = 0, \tag{2.5}$$

$$\nabla^2\psi + ieA^\beta\left(2\nabla_\beta + ieA_\beta\right)\psi + ie\nabla_\beta A^\beta\psi = 0, \tag{2.6}$$

$$\nabla^2\psi^* - ieA^\beta\left(2\nabla_\beta - ieA_\beta\right)\psi^* - ie\nabla_\beta A^\beta\psi^* = 0. \tag{2.7}$$

The derivation of the above equations of motion involved a conversion of the string frame into the Einstein frame, which are related via the conformal transformation

$$g_{\mu\nu} = e^{-2\phi}\hat{g}_{\mu\nu}, \tag{2.8}$$

where $g_{\mu\nu}$ and $\hat{g}_{\mu\nu}$ denote metric tensors in the Einstein and string frames, respectively [41]. The transformation between the two frames preserves causality. Since the obtained results will be mainly elaborated on employing notions related to causal structures of emerging spacetimes and features of the intrinsic dynamical objects, we do not expect the transformation to influence the ultimate conclusions and hence they can be regarded as physically relevant. From now on, all variables and quantities are written in the Einstein frame.

The gravitational field equations derived by varying the action (2.1) with respect to the metric tensor, taking the truncation of the theory into account, will complement the above set of equations describing the examined dynamical system. For the current studies, the double null spherically symmetric line element [42] is chosen

$$ds^2 = -a(u,v)^2 du dv + r^2(u,v) d\Omega^2, \tag{2.9}$$

where u and v are retarded and advanced time null coordinates, respectively, and $d\Omega^2 = d\Theta^2 + \sin^2\Theta d\Phi^2$ is the line element of the unit sphere, where Θ and Φ are angular coordinates. This choice of coordinates determines the spacetime foliation for conducting computations, which becomes 2+2 [43]. The double null formalism has been widely and successfully employed in dynamical gravitational collapse researches, e.g., [1,2,4,6–8]. Its advantage is that it enables to follow the dynamical evolution from approximately past null infinity, through the formation of possible horizons up to the final central singularity of singular spacetimes.

In spherical symmetry the only non-vanishing components of the electromagnetic field tensor are F_{uv} and F_{vu}. Due to the gauge freedom $A_u \to A_u + \nabla_u \theta'$, where $\theta' = \int A_v dv$, the only non-zero four-vector component is A_u. It is a function of retarded and advanced time.

The dilaton field equation of motion (2.4) in the chosen coordinate system is given by

$$\begin{aligned}
&r_{,u}\phi_{,v} + r_{,v}\phi_{,u} + r\phi_{,uv} - \alpha e^{2\alpha\phi}\frac{Q^2a^2}{4r^3} \\
&\quad + -\frac{\alpha+1}{8} r e^{2\phi(\alpha+1)} \\
&\quad \times \left[\psi_{,u}\psi^*_{,v} + \psi_{,v}\psi^*_{,u} + ieA_u\left(\psi\psi^*_{,v} - \psi^*\psi_{,v}\right)\right] \\
&\quad + -16\gamma\alpha e^{2\alpha\phi}\frac{1}{a^4 r} \\
&\quad \times \Big[12a_{,u}a_{,v}r_{,u}r_{,v} - 4a\left(a_{,v}r_{,v}r_{,uu} + a_{,u}r_{,u}r_{,vv}\right) \\
&\quad + 2a^2\left(r_{,uu}r_{,vv} - r^2_{,uv}\right) \\
&\quad - 4aa_{,uv}r_{,u}r_{,v} + a^2\left(a_{,u}a_{,v} - aa_{,uv}\right)\Big] = 0,
\end{aligned} \tag{2.10}$$

where we set

$$Q = 2\frac{A_{u,v}r^2}{a^2}. \tag{2.11}$$

Q is a function of retarded and advanced time and determines the electric charge within a sphere of a radius $r(u,v)$ on a spacelike hypersurface containing the point (u,v). Partial derivatives with respect to the null coordinates are marked as $_{,u}$ and $_{,v}$.

Concerning the assumed line element (2.9) and the definition of electric charge (2.11), the v-component of the Maxwell equations (2.5) can be written in the form describing dynamical behavior of the quantity Q, which is

$$Q_{,v} + 2\alpha\phi_{,v}Q + \frac{ier^2}{4}e^{2\phi}\left(\psi^*\psi_{,v} - \psi\psi^*_{,v}\right) = 0. \tag{2.12}$$

The evolution of the only non-zero component of the four-vector of the Maxwell field is governed by

$$A_{u,v} - \frac{Qa^2}{2r^2} = 0, \tag{2.13}$$

which stems from (2.11). The Eq. (2.12) can be rewritten in the form of a conservation law

$$\partial_v\left(e^{2\alpha\phi}Q\right) = j_v \quad \text{with} \quad j_v = -e^{2\alpha\phi}\frac{ier^2}{4}e^{2\phi}\left(\psi^*\psi_{,v} - \psi\psi^*_{,v}\right), \tag{2.14}$$

which indicates that the quantity $e^{2\alpha\phi}Q$ is conserved when the current associated with the complex scalar field vanishes. When the dilaton field also vanishes, Q is the quantity, which is conserved.

The equations for the complex scalar field (2.6)–(2.7) become

$$\begin{aligned}
&r_{,u}\psi_{,v} + r_{,v}\psi_{,u} + r\psi_{,uv} + ierA_u\psi_{,v} + ier_{,v}A_u\psi \\
&\quad + \frac{ieQa^2}{4r}\psi = 0,
\end{aligned} \tag{2.15}$$

$$\begin{aligned}
&r_{,u}\psi^*_{,v} + r_{,v}\psi^*_{,u} + r\psi^*_{,uv} - ierA_u\psi^*_{,v} - ier_{,v}A_u\psi^* \\
&\quad - \frac{ieQa^2}{4r}\psi^* = 0.
\end{aligned} \tag{2.16}$$

The stress-energy tensor for the considered electrically charged scalar field evolving within the decoupling limit of the dilaton–Gauss–Bonnet theory is the following:

$$\begin{aligned}
T_{\mu\nu} &= 2\phi_{,\mu}\phi_{,\nu} - g_{\mu\nu}\phi_{,\beta}\phi^{,\beta} \\
&\quad + e^{2\alpha\phi}\left(2F_{\mu\beta}F_{\nu}{}^{\beta} - \frac{1}{2}g_{\mu\nu}F_{\beta\sigma}F^{\beta\sigma}\right) - \frac{1}{4}e^{2\phi(\alpha+1)} \\
&\quad \times \Big[g_{\mu\nu}D_\beta\psi\left(D^\beta\psi\right)^* - D_\mu\psi\left(D_\nu\psi\right)^* \\
&\quad - \left(D_\mu\psi\right)^* D_\nu\psi\Big].
\end{aligned} \tag{2.17}$$

Its non-vanishing components written in double null coordinates are

$$T_{uu} = 2\phi_{,u}^2 + \frac{1}{2}e^{2\phi(\alpha+1)} \times \left[\psi_{,u}\psi_{,u}^* + ieA_u\left(\psi\psi_{,u}^* - \psi^*\psi_{,u}\right) + e^2A_u^2\psi\psi^*\right], \tag{2.18}$$

$$T_{vv} = 2\phi_{,v}^2 + \frac{1}{2}e^{2\phi(\alpha+1)}\psi_{,v}\psi_{,v}^*, \tag{2.19}$$

$$T_{uv} = e^{2\alpha\phi}\frac{Q^2a^2}{2r^4}, \tag{2.20}$$

$$T_{\theta\theta} = 4\frac{r^2}{a^2}\phi_{,u}\phi_{,v} + e^{2\alpha\phi}\frac{Q^2}{r^2} + \frac{1}{2}\frac{r^2}{a^2}e^{2\phi(\alpha+1)} \times \left[\psi_{,u}\psi_{,v}^* + \psi_{,v}\psi_{,u}^* + ieA_u\left(\psi\psi_{,v}^* - \psi^*\psi_{,v}\right)\right]. \tag{2.21}$$

Combining the adequate components of the Einstein tensor resulting from the metric (2.9) and the obtained stress-energy tensor components, the Einstein equations yield

$$\frac{2a_{,u}r_{,u}}{a} - r_{,uu} = r\phi_{,u}^2 + \frac{r}{4}e^{2\phi(\alpha+1)} \times \left[\psi_{,u}\psi_{,u}^* + ieA_u\left(\psi\psi_{,u}^* - \psi^*\psi_{,u}\right) + e^2A_u^2\psi\psi^*\right], \tag{2.22}$$

$$\frac{2a_{,v}r_{,v}}{a} - r_{,vv} = r\phi_{,v}^2 + \frac{r}{4}e^{2\phi(\alpha+1)}\psi_{,v}\psi_{,v}^*, \tag{2.23}$$

$$\frac{a^2}{4r} + \frac{r_{,u}r_v}{r} + r_{,uv} = e^{2\alpha\phi}\frac{Q^2a^2}{4r^3}, \tag{2.24}$$

$$\frac{a_{,u}a_{,v}}{a^2} - \frac{a_{,uv}}{a} - \frac{r_{,uv}}{r} = e^{2\alpha\phi}\frac{Q^2a^2}{4r^4} + \phi_{,u}\phi_{,v} + \frac{1}{8}e^{2\phi(\alpha+1)}\Big[\psi_{,u}\psi_{,v}^* + \psi_{,u}^*\psi_{,v} + ieA_u\left(\psi\psi_v^* - \psi^*\psi_{,v}\right)\Big]. \tag{2.25}$$

They complement the matter equations presented above in order to obtain the complete set of equations describing the dynamics of the examined system, which are (2.10)–(2.16), without the relation (2.11), which is a definition of the physical quantity Q.

The following set of auxiliary variables is introduced to prepare the obtained set of dynamical equations to be solved numerically:

$$c = \frac{a_{,u}}{a}, \quad d = \frac{a_{,v}}{a}, \quad f = r_{,u}, \quad g = r_{,v},$$
$$h = \phi, \quad x = \phi_{,u}, \quad y = \phi_{,v},$$
$$s = \psi, \quad p = \psi_{,u}, \quad q = \psi_{,v}, \quad \beta = A_u. \tag{2.26}$$

It is supplemented by the quantities

$$\lambda \equiv \frac{a^2}{4} + fg, \quad \mu \equiv fq + gp, \quad \eta \equiv gx + fy. \tag{2.27}$$

The above variables make it possible to rewrite the second-order differential equations (2.10), (2.15)–(2.16) and (2.22)–(2.25) as first-order ones. Additionally, real fields ψ_1 and ψ_2 are introduced instead of conjugate fields ψ and ψ^* according to relations $\psi = \psi_1 + i\psi_2$, $\psi^* = \psi_1 - i\psi_2$, what results in

$$s = s_1 + is_2, \quad p = p_1 + ip_2, \quad q = q_1 + iq_2,$$
$$\mu = \mu_1 + i\mu_2, \quad \mu_1 = fq_1 + gp_1, \quad \mu_2 = fq_2 + gp_2. \tag{2.28}$$

After introducing the above substitutions, the final system of equations of motion describing the gravitational collapse of interest can be written as

$$P1: \quad a_{,u} = ac, \tag{2.29}$$
$$P2: \quad a_{,v} = ad, \tag{2.30}$$
$$P3: \quad r_{,u} = f, \tag{2.31}$$
$$P4: \quad r_{,v} = g, \tag{2.32}$$
$$P5: \quad s_{1(2),u} = p_{1(2)}, \tag{2.33}$$
$$P6: \quad s_{1(2),v} = q_{1(2)}, \tag{2.34}$$
$$P7: \quad h_{,u} = x, \tag{2.35}$$
$$P8: \quad h_{,v} = y, \tag{2.36}$$
$$E1: \quad f_{,u} = 2cf - rx^2 - \frac{r}{4}e^{2h(\alpha+1)} \left[p_1^2 + p_2^2 + 2e\beta\left(s_1p_2 - s_2p_1\right) + e^2\beta^2\left(s_1^2 + s_2^2\right)\right], \tag{2.37}$$
$$E2: \quad g_{,v} = 2dg - ry^2 - \frac{r}{4}e^{2h(\alpha+1)}\left(q_1^2 + q_2^2\right), \tag{2.38}$$
$$E3: \quad g_{,u} = f_{,v} = -\frac{\lambda}{r} + e^{2\alpha h}\frac{Q^2a^2}{4r^3}, \tag{2.39}$$
$$E4: \quad d_{,u} = c_{,v} = \frac{\lambda}{r^2} - xy - \frac{1}{4}e^{2h(\alpha+1)} \left[p_1q_1 + p_2q_2 + e\beta\left(s_1q_2 - s_2q_1\right)\right] - e^{2\alpha h}\frac{Q^2a^2}{2r^4}, \tag{2.40}$$
$$S_{(Re)}: \quad q_{1,u} = p_{1,v} = -\frac{\mu_1}{r} + e\beta q_2 + es_2\beta\frac{g}{r} + es_2\frac{Qa^2}{4r^2}, \tag{2.41}$$
$$S_{(Im)}: \quad q_{2,u} = p_{2,v} = -\frac{\mu_2}{r} - e\beta q_1 - es_1\beta\frac{g}{r} - es_1\frac{Qa^2}{4r^2}, \tag{2.42}$$
$$M1: \quad \beta_{,v} = \frac{Qa^2}{2r^2}, \tag{2.43}$$
$$M2: \quad Q_{,v} = -2\alpha yQ + \frac{er^2}{2}e^{2h}\left(s_1q_2 - s_2q_1\right), \tag{2.44}$$
$$D: \quad y_{,u} = x_{,v} = -\frac{\eta}{r} + \alpha e^{2\alpha h}\frac{Q^2a^2}{4r^4} \left[1 + \frac{32}{a^2r}\gamma e^{2\alpha h}\left(6\lambda - e^{2\alpha h}\frac{Q^2a^2}{4r^2}\right)\right]$$

$$+\left(\frac{\alpha+1}{4}+\frac{16}{a^2 r}\lambda\gamma\alpha e^{2\alpha h}\right)e^{2h(\alpha+1)}$$
$$\left[p_1 q_1+p_2 q_2+e\beta\left(s_1 q_2-s_2 q_1\right)\right]$$
$$+\frac{32}{a^2 r}\gamma\alpha e^{2\alpha h}\left\{\lambda\left(2xy-3\frac{\lambda}{r^2}\right)\right.$$
$$+r^2\left[x^2y^2+\frac{x^2}{4}e^{2h(\alpha+1)}\left(q_1^2+q_2^2\right)\right.$$
$$\left.+\frac{1}{4}e^{2h(\alpha+1)}\left(y^2+\frac{1}{4}e^{2h(\alpha+1)}\left(q_1^2+q_2^2\right)\right)\right.$$
$$\left.\left.\cdot\left[p_1^2+p_2^2+2e\beta\left(s_1 p_2-s_2 p_1\right)+e^2\beta^2\left(s_1^2+s_2^2\right)\right]\right]\right\}. \tag{2.45}$$

3 Details of numerical simulations and results analysis

The obtained complex coupled system of differential equations (2.29)–(2.45) does not possess an analytic solution and needs to be solved numerically. The prepared code and tests run to confirm its correctness are presented in Appendix A.

The equations describing the dynamics of the considered systems were solved in the bounded region of the (vu)-plane. It is shown in Fig. 1 on the background of a dynamical Schwarzschild spacetime, whose Carter-Penrose diagram does not differ from the static case. The borders of the computational domain were marked for numerical purposes as 0 and 7.5 in the v-direction, 0 and 15 in the u-direction in all conducted simulations. The only arbitrary data of the numerical computations were initial profiles of the evolving fields, posed on the null hypersurface denoted as $u = 0$. This initial hypersurface was assumed to be a Minkowski spacetime with zero mass and charge. In order to describe the behavior of the real and complex scalar fields properly, their initial profiles were of the following Gaussian and trigonometric types, respectively, [3,4,6,44]:

$$h=\tilde{p}_h\cdot v^2\cdot e^{-\left(\frac{v-c_1}{c_2}\right)^2}, \tag{3.1}$$
$$s=\tilde{p}_s\cdot\sin^2\left(\pi\frac{v}{v_f}\right)\cdot\left[\cos\left(\pi\frac{2v}{v_f}\right)+i\cos\left(\pi\frac{2v}{v_f}+\delta\right)\right]. \tag{3.2}$$

The profiles were one-parameter families with amplitudes $\tilde{p}_h$ and $\tilde{p}_s$ being the free family parameters. The amplitudes determine the strength of the gravitational self-interaction of the particular field [45]. The remaining arbitrary constants were invariable during computations, precisely $c_1 = 1.3$, $c_2 = 0.21$ and the parameter that controls the amount of initial charge $\delta = \frac{\pi}{2}$. The final value of advanced time was $v_f = 2.5$. The initial conditions are representative for the conducted evolutions, as their outcomes do not depend of the profiles types provided that they are regular, what means that they result in a regular spacetime slice at the initial $u =$ *const* hypersurface. This condition is fulfilled by the above profiles (3.1) and (3.2).

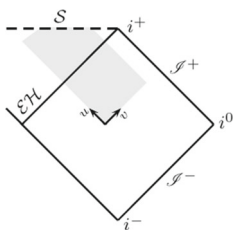

Fig. 1 The computational domain (marked gray) on the background of a dynamical Schwarzschild spacetime shown on the Carter-Penrose diagram. The central singularity along $r = 0$ and the event horizon are denoted as $\mathcal{S}$ and $\mathcal{EH}$, respectively. $\mathscr{I}^{\pm}$ and $i^{\pm}$ are null and timelike infinities, respectively, i^0 is a spacelike infinity

When the value of the electric coupling constant is not equal to zero, it does not affect the results of the collapse [13]. It was confirmed for the investigated cases. Thus e was set as equal to 1 in all evolutions. The case of a vanishing electric coupling constant is beyond the scope of the current research, as it comes down to an analysis of two neutral fields instead of one electrically charged in the spacetime.

The values of the remaining model parameters, i.e., α and γ were assigned as follows. The dilatonic coupling constant was equal to $-\sqrt{3}$, -1 and 0, while γ was taken from within the range $\langle -1, 1\rangle$. The values of α corresponded to the dimensionally reduced Kaluza–Klein theory, dilaton gravity and the Einstein–Maxwell theory. The range of γ was consistent with observational constraints (for a thorough analysis see [34] and references therein).

The spacetime structures resulting from the dynamical evolutions of interest will be presented on Penrose diagrams, which contain contours of $r = const$ lines plotted in the (vu)-plane. The outermost line refers to $r = 0$, which in all presented cases will be a part of a central singularity. The lines indicating the vanishing expansion

$$\theta_v \equiv \frac{2}{r}r_{,v} \tag{3.3}$$

will be also presented on the diagrams and they will indicate the location of an apparent horizon in the spacetime. On the spacetime diagrams they will be marked as red solid lines. On the remaining plots they will be marked in black. An apparent horizon coincides with an event horizon in a spacetime region where it settles along a null hypersurface. The locations of thus located event horizons were shown on the spacetime diagrams as blue solid lines.

One of physical quantities which was employed in the interpretation of the obtained results is the quasi-local Hawking mass [46]. Its value calculated for the spherically symmetric spacetime with a gauge field A_μ is the following:

$$m(u,v)=\frac{r}{2}\left(1+\frac{4fg}{a^2}+\frac{Q^2}{r^2}\right). \tag{3.4}$$

It describes the amount of mass contained within a sphere of a radius $r(u, v)$ on a spacelike hypersurface containing the particular point (u, v). The mass of a singular object can be expressed by a value of the above expression calculated at the event horizon in the region of the emerging spacetime which is not dynamical, that is for large values of advanced time.

The outcomes of the gravitational collapse within the discussed model were also inspected with the use of a set of local spacetime quantities that may be interpreted as observables related with an observer moving with the evolving matter. The analysed quantities were energy density $\hat{\rho}$, radial pressure $\hat{p}_r$ and pressure anisotropy $\hat{p}_a \equiv \hat{p}_t - \hat{p}_r$, where $\hat{p}_t$ denotes tangential pressure. Their precise covariant derivation for any general case can be found in [27]. Moreover, local temperature $T_l = \frac{\kappa_l}{2\pi}$ with the surface gravity defined as $\kappa_l = a_{,u} a^{-2}$ [47,48] was also calculated. For the studied gravity–matter model considered in double null coordinates the first three of the above observables are given by relations

$$\begin{aligned}\hat{\rho} = {} & e^{2\alpha h}\frac{Q^2}{r^4} + \frac{1}{2a^2} \\ & \times \left[4\left(x^2+y^2\right) + e^{2h(\alpha+1)}\left(p_1^2+p_2^2+q_1^2+q_2^2\right)\right. \\ & + 2\beta e^{[2h(\alpha+1)+1]}\left(s_1 p_2 - s_2 p_1\right) \\ & \left. +\beta^2 e^{2[h(\alpha+1)+1]}\left(s_1^2+s_2^2\right)\right], \end{aligned} \tag{3.5}$$

$$\begin{aligned}\hat{p}_r = {} & -e^{2\alpha h}\frac{Q^2}{r^4} + \frac{1}{2a^2} \\ & \times \left[4\left(x^2+y^2\right) + e^{2h(\alpha+1)}\left(p_1^2+p_2^2+q_1^2+q_2^2\right)\right. \\ & + 2\beta e^{[2h(\alpha+1)+1]}\left(s_1 p_2 - s_2 p_1\right) \\ & \left. +\beta^2 e^{2[h(\alpha+1)+1]}\left(s_1^2+s_2^2\right)\right], \end{aligned} \tag{3.6}$$

$$\begin{aligned}\hat{p}_a = {} & 2e^{2\alpha h}\frac{Q^2}{r^4} - \frac{1}{2a^2}\left\{4\left(x-y\right)^2 + e^{2h(\alpha+1)}\right. \\ & \times \left[\left(p_1-q_1\right)^2 + \left(p_2-q_2\right)^2\right] \\ & + 2\beta e^{[2h(\alpha+1)+1]}\left(s_1 p_2 - s_1 q_2 - s_2 p_1 + s_2 q_1\right) \\ & \left. +\beta^2 e^{2[h(\alpha+1)+1]}\left(s_1^2+s_2^2\right)\right\}. \end{aligned} \tag{3.7}$$

4 Dynamical spacetime structures

The spacetimes which emerge during the investigated collapse are either non-singular, for small values of the field self-interaction strengths, or singular, containing in all cases a dynamical black hole of a Schwarzschild type, for sufficiently big self-interactions represented by values of field amplitudes. The singular spacetimes resulting from dynamical evolutions within the model of interest for a few values of the field amplitudes were presented for several combinations of the model parameters, that is $\alpha = -\sqrt{3}$ and $\gamma = -0.01$, $\alpha = -1$ and $\gamma = -1$, $\alpha = -1$ and $\gamma = 1$ and $\alpha = 0$ and $\gamma = -0.1$, in Figs. 2, 3, 4 and 5, respectively.

Each resulting dynamical Schwarzschild spacetime contains a central spacelike singularity located along the $r = 0$ line. It is indicated by the outermost $r = const$ line on the Penrose diagram. The singularity is surrounded by a single apparent horizon located along the $r_{,v} = 0$ line, whose behavior divides the whole spacetime into two regions, i.e., a dynamical one, within which the actual collapse proceeds, and a non-dynamical one, remaining after the dynamical evolution. The former corresponds to the range of small values of advanced time, in which the apparent horizon is spacelike and changes its location in the u-coordinate. The latter region refers to the v-range of big values, where $v \to \infty$ and the apparent horizon settles along a null hypersurface

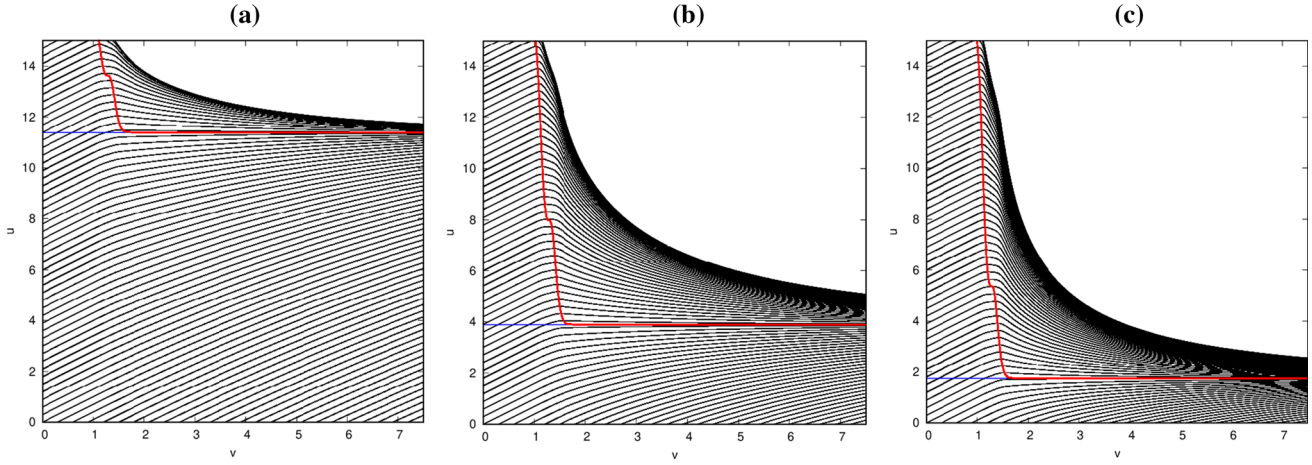

Fig. 2 Penrose diagrams of spacetimes emerging from evolutions with $\alpha = -\sqrt{3}$ and $\gamma = -0.01$. The field amplitudes $\tilde{p}_s = \tilde{p}_h$ were equal to **a** 0.02, **b** 0.04 and **c** 0.05

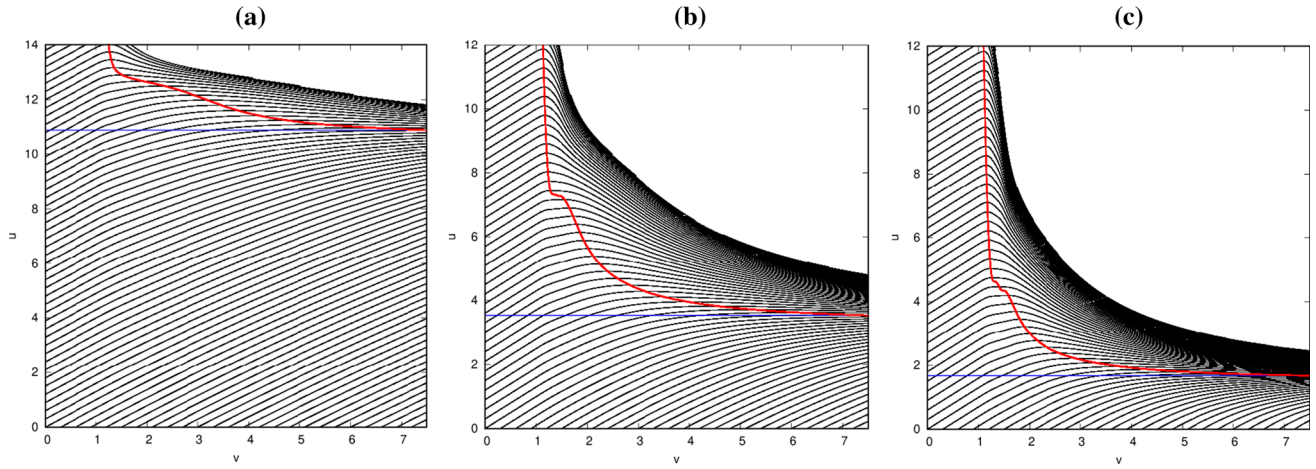

Fig. 3 Penrose diagrams of spacetimes emerging from evolutions with $\alpha = -1$ and $\gamma = -1$. The field amplitudes $\tilde{p}_s = \tilde{p}_h$ were equal to **a** 0.02, **b** 0.04 and **c** 0.05

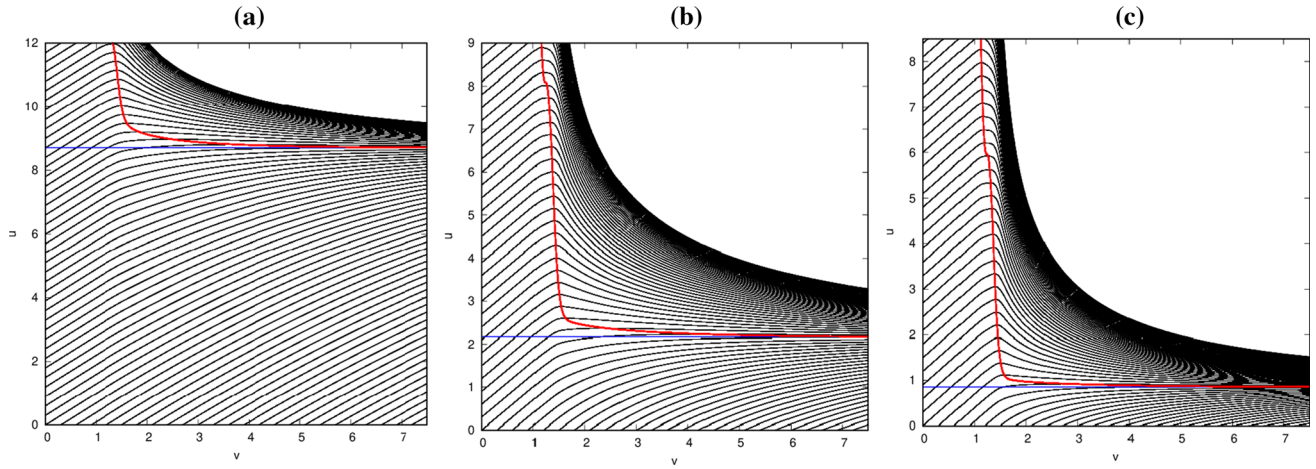

Fig. 4 Penrose diagrams of spacetimes emerging from evolutions with $\alpha = -1$ and $\gamma = 1$. The field amplitudes $\tilde{p}_s = \tilde{p}_h$ were equal to **a** 0.02, **b** 0.04 and **c** 0.05

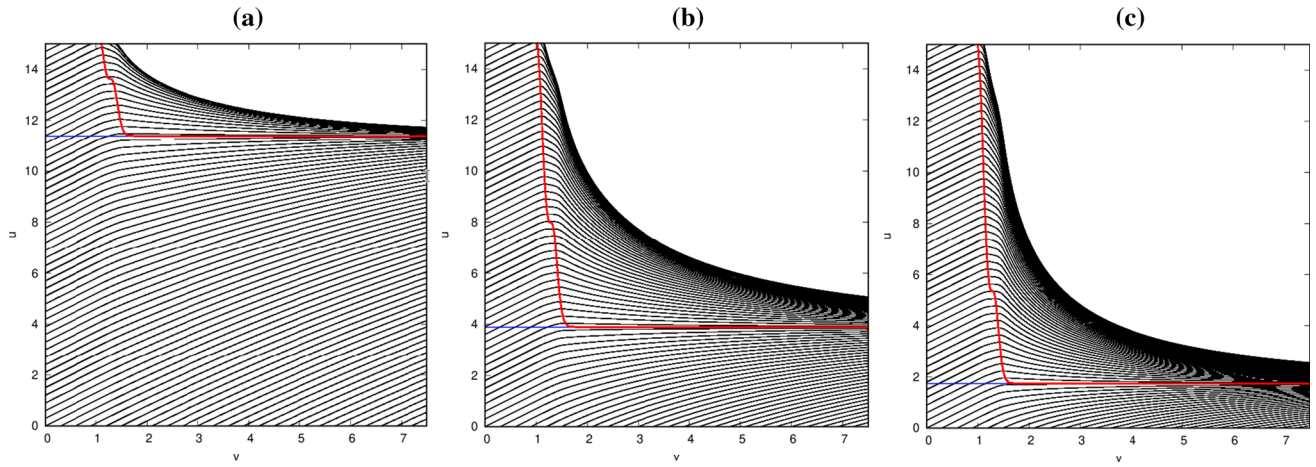

Fig. 5 Penrose diagrams of spacetimes emerging from evolutions with $\alpha = 0$ and $\gamma = -0.1$. The field amplitudes $\tilde{p}_s = \tilde{p}_h$ were equal to **a** 0.02, **b** 0.04 and **c** 0.05

of constant retarded time, thus indicating the location of the event horizon in spacetime.

The analysis of the behavior of the apparent horizons in the presented cases allows to draw a conclusion that the value of $|\gamma|$ influences the size of a dynamical region within the evolving spacetime. For small absolute values of the coupling the location of the horizon changes significantly within a small range of the v-coordinate and it immediately settles along a constant-u null hypersurface, where it coincides with the event horizon. When the absolute value of γ gets bigger, the region in which the dynamics is observed extends much farther in the v-direction and the horizon settles along a null hypersurface of constant retarded time much later in terms of advanced time. The transition between the spacelike and null portions of the horizon is less sharp in this case. The evident dependence of the time of formation of a black hole and its size on the value of the evolving fields amplitudes will be discussed in detail in Sect. 5.

5 Collapse characteristics

The examined collapse characteristics were the u-locations of the event horizons, radii, masses and electric charges of black holes formed during the gravitational evolutions within the model of interest. They were examined as functions of the model couplings $\alpha\epsilon\langle-\sqrt{3}, \sqrt{3}\rangle$ and $\gamma\epsilon\langle-1, 1\rangle$, as well as field amplitudes $\tilde{p}_s = \tilde{p}_h\epsilon\langle 0.01, 0.09\rangle$ for a selected evolution characterized by the following parameters: $\alpha = -1$, $\gamma = 1$, $\tilde{p}_s = \tilde{p}_h = 0.04$. When the dependence on the specific parameter of the model is presented, the remaining ones are as listed above. In the case of the dependency on the field self-interaction strengths, several combinations of the model parameters were considered.

The dependencies of the abovementioned characteristics on the model parameters are presented in Figs. 6 and 7. The dependencies of the u-locations of the event horizons, radii and masses on both α and γ are in both cases qualitatively the same, that is there exist a maximum for u^{eh} at $\alpha = 0.25$ and $\gamma = -0.2$ and minima at $\alpha = 0.1$ and

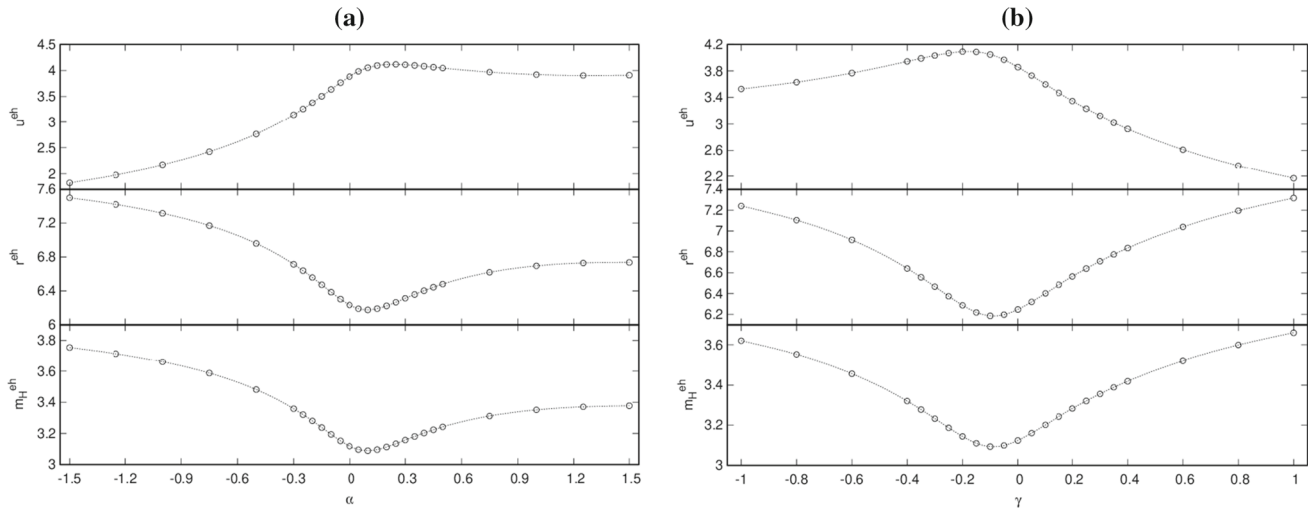

Fig. 6 The u-locations of the event horizons, u^{eh}, radii, r^{eh}, and masses, m_H^{eh}, of black holes formed during the gravitational collapse as functions of **a** α and **b** γ. The non-varying parameters were $\alpha = -1$ for (**b**), $\gamma = 1$ for (**a**) and $\tilde{p}_s = \tilde{p}_h = 0.04$

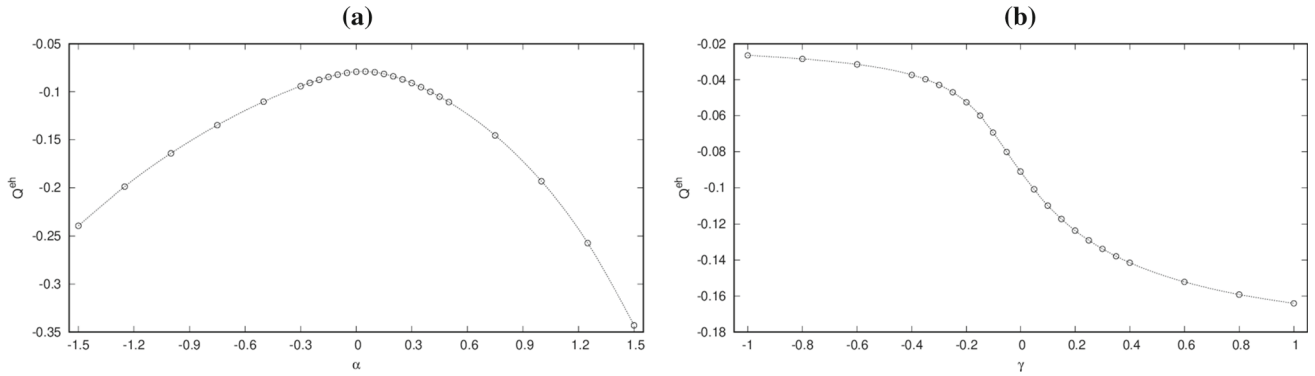

Fig. 7 The black hole charge related to the $U(1)$ gauge field, Q^{eh}, as function of **a** α and **b** γ, for non-varying parameters as in Fig. 6

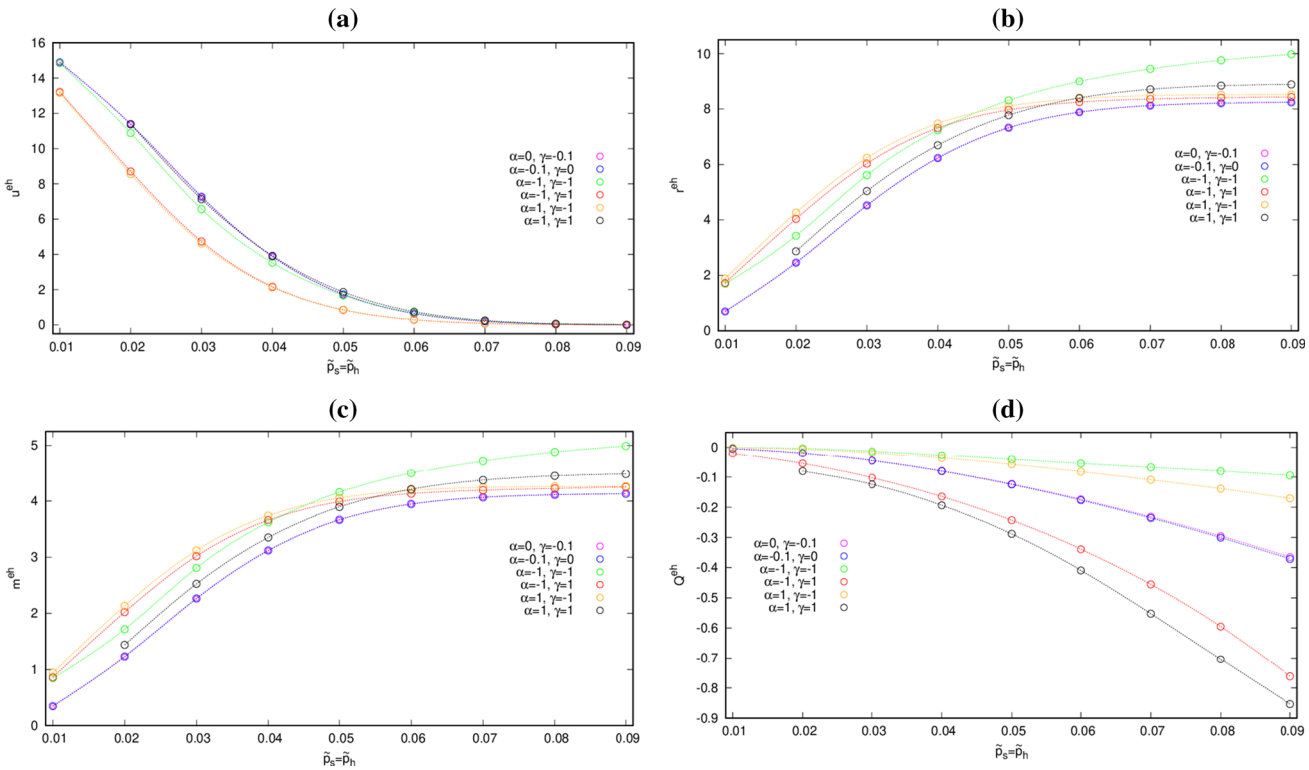

Fig. 8 The **a** u-locations of the event horizons, u^{eh}, **b** radii, r^{eh}, **c** masses, m_H^{eh}, and **d** charges related to the $U(1)$ gauge field, Q^{eh}, of black holes formed during the gravitational collapse as functions of the field amplitudes, $\tilde{p}_s$ and $\tilde{p}_h$, for several combinations of values of the parameters α and γ

$\gamma = -0.1$ for the remaining characteristics. The black hole electric charge increases for small values of the dilatonic coupling constant up to an extremum $\alpha = 0.05$ and decreases for its larger values. Q^{eh} decreases monotonically with an increasing γ.

Figure 8 presents the discussed characteristics as functions of the collapsing fields amplitudes for several combinations of the couplings present within the studied model. In all cases, for increasing field self-interaction strengths the changes of the characteristics are monotonic. The u-locations of the event horizons and black hole electric charges decrease, while radii and masses of the forming singular objects increase with increasing $\tilde{p}_s = \tilde{p}_h$. The changes of u^{eh}, r^{eh} and m_H^{eh} become smaller with increasing field amplitudes. An opposite tendency is observed for Q^{eh}.

6 Observables and fields

The (vu)-distributions of observables presented in Sect. 3 and the evolving scalar fields, along with the relation between local temperature along the apparent horizon and the v-coordinate will be shown and discussed for selected spacetimes, the structures of which were shown in Sect. 4. Additionally, the distribution of tangential to radial pressures ratio will be shown in order to investigate the pressure anisotropy in more detail.

Figures 9 and 10 present the considered spacetime distributions for the spacetime whose structure was shown in Fig. 2b, with the model parameters $\alpha = -\sqrt{3}$ and $\gamma = -0.01$. The highest absolute values of the discussed observables as well as both the neutral and the moduli of the complex scalar field functions are located along a constant-v null direction, which is a direction of peaks of initially imposed field functions propagation. A considerable increase in their values appears as the central singularity is approached. This increase is observed only within the range of advanced time, in which the highest field values were imposed initially. The energy density, radial pressure and the moduli of the complex scalar field are positive within the whole integration domain. On the contrary, the pressure anisotropy and the neutral scalar field function are negative there. The ratio between tangential and radial pressures indicates that the pressure anisotropy is dominated by the $\hat{p}_r$ component within most spacetime regions. Both components of $\hat{p}_a$ are of the same order in the vicinity of the singularity and along the null $v = const$ direction of propagation of the highest initial values of the imposed field functions for large retarded time. The black hole local temperature calculated along the apparent horizon is positive and it increases with advanced time.

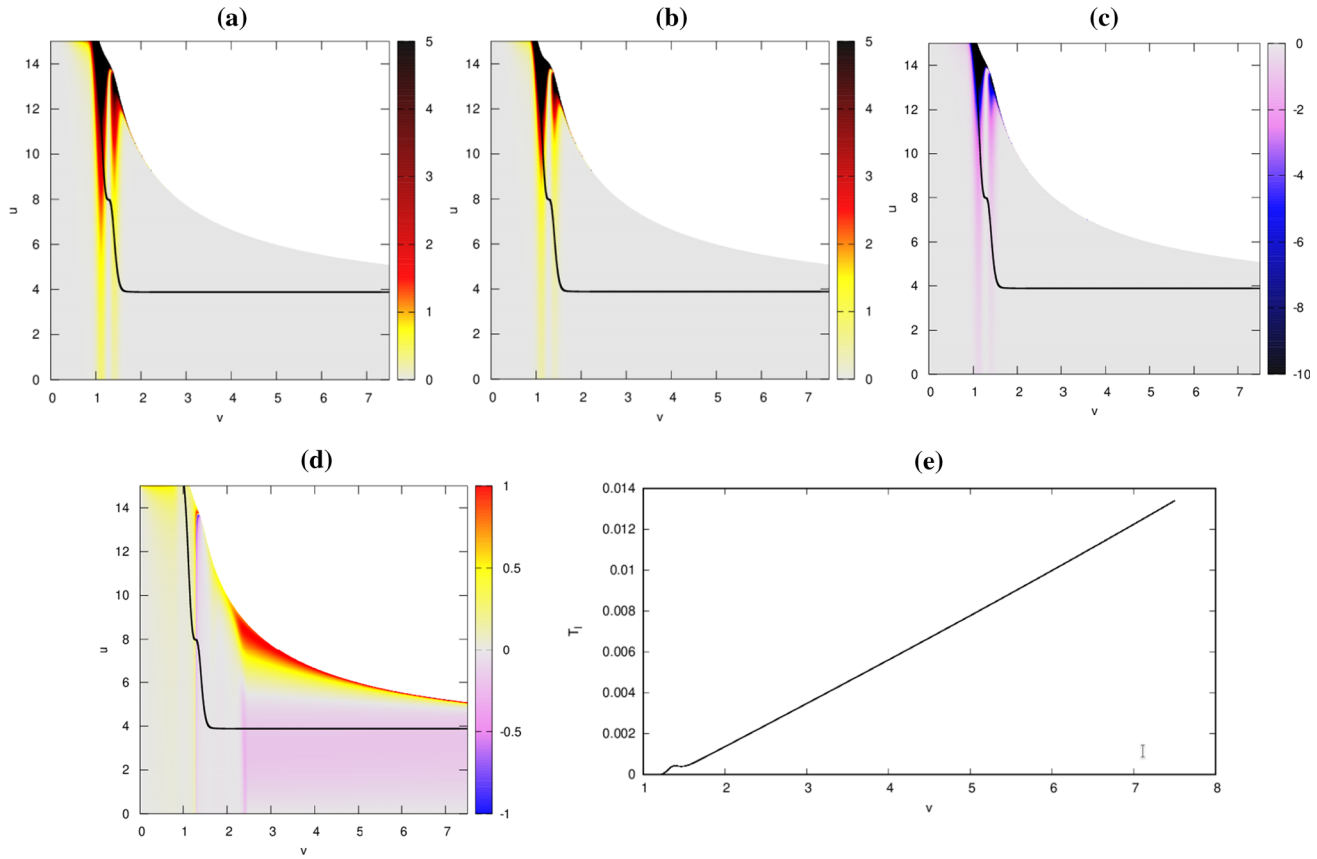

Fig. 9 The (vu)-distribution of **a** energy density, $\hat{\rho}$, **b** radial pressure, $\hat{p}_r$, **c** pressure anisotropy, $\hat{p}_a$, **d** tangential to radial pressures ratio, $\frac{\hat{p}_t}{\hat{p}_r}$, and **e** local temperature along the black hole apparent horizon, T_l, as a function of advanced time for a dynamical evolution characterized by parameters $\alpha = -\sqrt{3}$, $\gamma = -0.01$ and $\tilde{p}_s = \tilde{p}_h = 0.04$ (the same as in Fig. 2b)

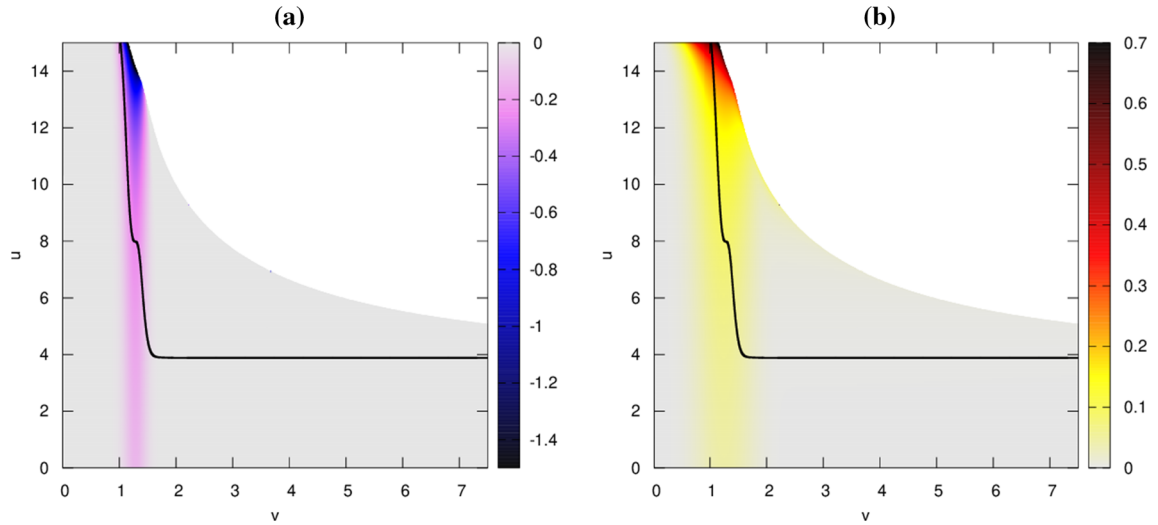

Fig. 10 The (vu)-distribution of **a** the neutral scalar field, h, and **b** the moduli of the complex scalar field, $|s|$, for the same parameters and field amplitudes as in Fig. 9

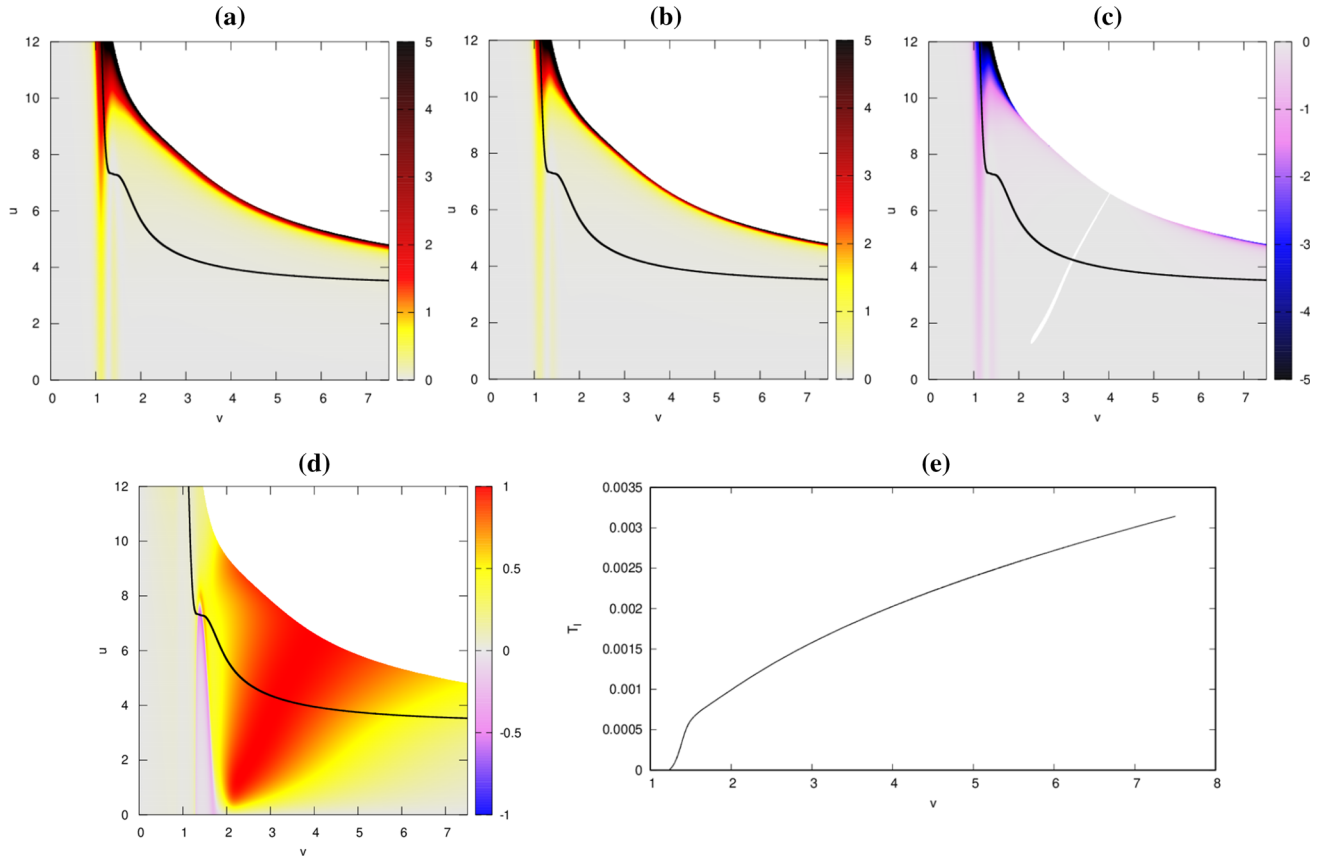

Fig. 11 The (vu)-distribution of **a** energy density, $\hat{\rho}$, **b** radial pressure, $\hat{p}_r$, **c** pressure anisotropy, $\hat{p}_a$, **d** tangential to radial pressures ratio, $\frac{\hat{p}_t}{\hat{p}_r}$, and **e** local temperature along the black hole apparent horizon, T_l, as a function of advanced time for a dynamical evolution characterized by parameters $\alpha = -1$, $\gamma = -1$ and $\tilde{p}_s = \tilde{p}_h = 0.04$ (the same as in Fig. 3b)

The changes are not monotonic. It increases for small values of the v-coordinate, reaches a maximum within the v-range, where there exists a small inclination of the apparent horizon and then, after a slight decrease, it increases monotonically in a nearly linear manner.

The distributions of observables and field functions resulting from the evolution leading to the spacetime with the structure shown in Fig. 3b, obtained with $\alpha = -1$ and $\gamma = -1$, are presented in Figs. 11 and 12, respectively. As in the case discussed above, the energy density and the moduli of the complex scalar field are positive, while the pressure anisotropy and the neutral scalar field function are negative within the whole domain of integration. What distinguishes this case from the other discussed is the fact that non-zero energy density and radial pressure persist also for large values of advanced time. Moreover, pressure anisotropy is also non-zero for large v. This implies that there is a persisting non-trivial matter distribution around the central singularity. This observation finds its confirmation in Fig. 12a. The dilaton field does not collapse completely but instead attains a non-zero value even outside the black hole event horizon. This may indicate that in this case a formation of a hairy black hole is observed. Additionally, the domination of the $\hat{p}_r$ component of the pressure anisotropy over $\hat{p}_t$ is less spread in the spacetime than in the previous case. It is observed within the highly dynamical spacetime region, that is for small values of advanced time and for small values of retarded time for large v. In the remaining locations the values of the two components of $\hat{p}_a$ are comparable. The local temperature in the examined case is positive and increases monotonically with advanced time along the apparent horizon with a slight inclination in the region, where an inclination of the apparent horizon is also visible. Unlike the case depicted in Fig. 13e, the late-lime increase is not linear.

The distributions of the discussed quantities, that is observables and field functions, for the evolution with the emerging spacetime structure presented in Fig. 4b, resulting from the evolution with $\alpha = -1$ and $\gamma = 1$, are shown in Figs. 13 and 14. The signs of the particular quantities are the same as in the cases presented above. An increase of absolute values of the observables is visible in the region corresponding to advanced time where the field values was the

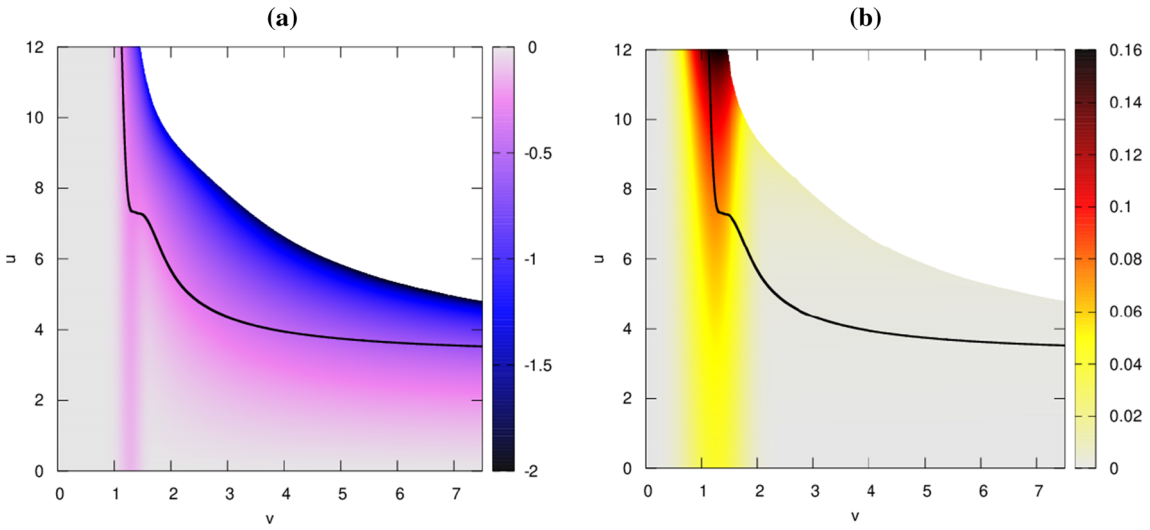

Fig. 12 The (vu)-distribution of **a** the neutral scalar field, h, and **b** the moduli of the complex scalar field, $|s|$, for the same parameters and field amplitudes as in Fig. 11

highest initially. The energy density, radial pressure and pressure anisotropy also display an increase in values nearby the central singularity, and the distribution of values of the tangential to radial pressures ratio displays a specific triangular shape within the spacetime, as in the latter of the above cases. The local temperature along the black hole apparent horizon behaves like in the first case above, namely it increases for small values of v, then, after reaching a maximum it slightly decreases and the decrease turns into the late-time nearly linear increase as $v \to \infty$.

The spacetime distribution of the analysed observables and fields for the evolution with $\alpha = 0$ and $\gamma = -0.1$, with the structure of spacetime shown in Fig. 5b, presented in Figs. 15 and 16, is analogous to the one presented above for the case of $\alpha = -\sqrt{3}$ and $\gamma = -0.01$. The energy density, radial pressure and the moduli of the complex scalar field are positive, while the pressure anisotropy and the neutral scalar field function are negative within the dynamical spacetime region covered by numerical calculations. A sole increase in absolute values in all the distributions is visible along the null $v = const$ direction of propagation of the highest initial values of the imposed field functions. The distribution of values of the tangential to radial pressures ratio reveals that there exists a spacelike cut-off, which sets a border between two regions in which for small advanced times $\hat{p}_r$ dominates, while for large advanced times the two components of $\hat{p}_a$ are of the same order. In the low-v region, there also exist locations, in which $\hat{p}_t$ and $\hat{p}_r$ are comparable, for large retarded times, similarly to the first of the cases discussed above. The changes in values of the local temperature calculated along the black hole apparent horizon tend to a late-time increase close to linear, after reaching a shallow extrema, precisely a maximum and a minimum for small values of advanced time in the range where an inclination of the apparent horizon appears.

7 Conclusions

The course and outcomes of gravitational evolutions involving electric charge in a decoupling limit of the dilatonic Gauss–Bonnet gravity was investigated. The system consisted of two scalar fields, namely a neutral scalar dilaton field and a complex scalar field coupled with a $U(1)$ gauge field, i.e., electrically charged. The dilaton was coupled both with the matter and Gauss–Bonnet sectors of the theory.

The course of the dynamical collapse was traced numerically. The formation of dynamical spacetimes and emerging black holes was observed and analysed via description of spacetime structures, inspection of the collapse characteristics and values of gravitational observables and evolving fields within the forming spacetimes.

The collapse resulted in either non-singular spacetimes formed for small self-interaction strengths of the fields, that is small initial values of their amplitudes, or singular spacetimes containing black holes. The particular spacetime contained a central spacelike singularity along $r = 0$ surrounded by a single apparent horizon, which was spacelike in the dynamical region, i.e., for small values of advanced time, and became null as $v \to \infty$. Disregarding the values of the model parameters α and γ, the black holes were of a Schwarzschild type, despite the fact that the evolving scalar field was electrically charged. Such a situation was observed in the case of a dynamical gravitational collapse of an electrically charged scalar field in dilaton gravity, but only for non-zero values of the dilatonic coupling constant [13]. Taking this into account,

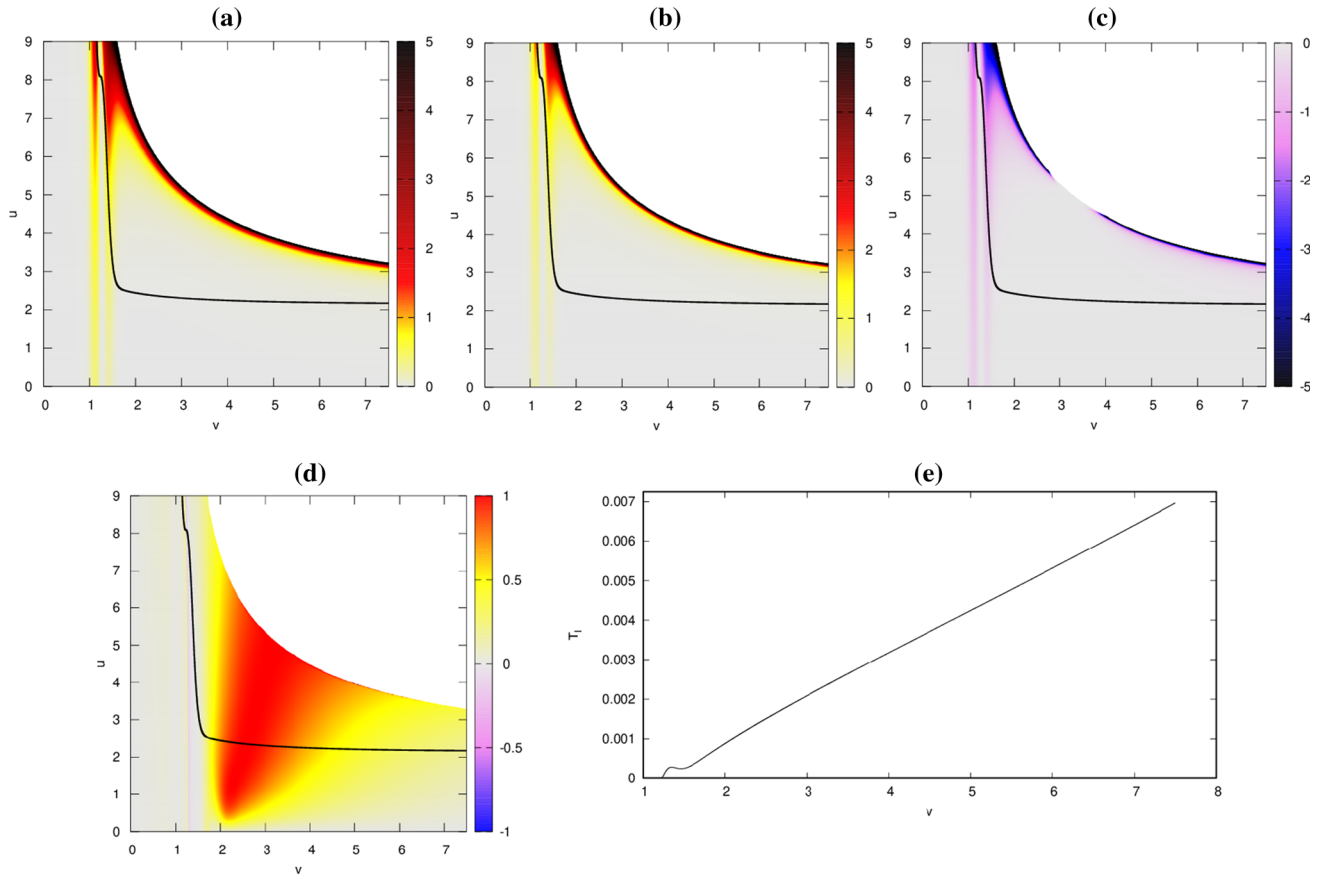

Fig. 13 The (vu)-distribution of **a** energy density, $\hat{\rho}$, **b** radial pressure, $\hat{p}_r$, **c** pressure anisotropy, $\hat{p}_a$, **d** tangential to radial pressures ratio, $\frac{\hat{p}_t}{\hat{p}_r}$, and **e** local temperature along the black hole apparent horizon, T_l, as a function of advanced time for a dynamical evolution characterized by parameters $\alpha = -1$, $\gamma = 1$ and $\tilde{p}_s = \tilde{p}_h = 0.04$ (the same as in figure 4(b))

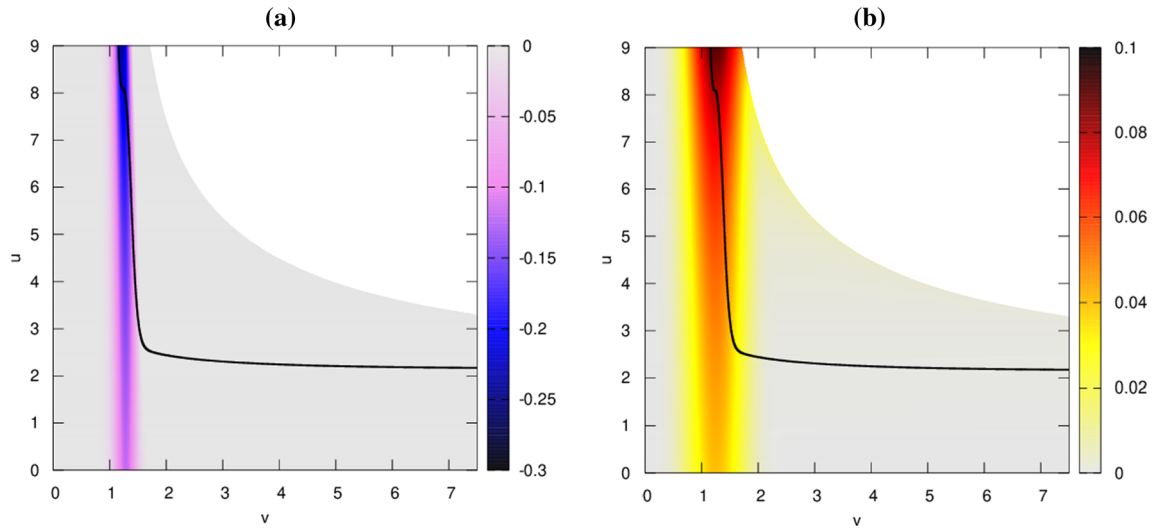

Fig. 14 The (vu)-distribution of **a** the neutral scalar field, h, and **b** the moduli of the complex scalar field, $|s|$, for the same parameters and field amplitudes as in Fig. 13

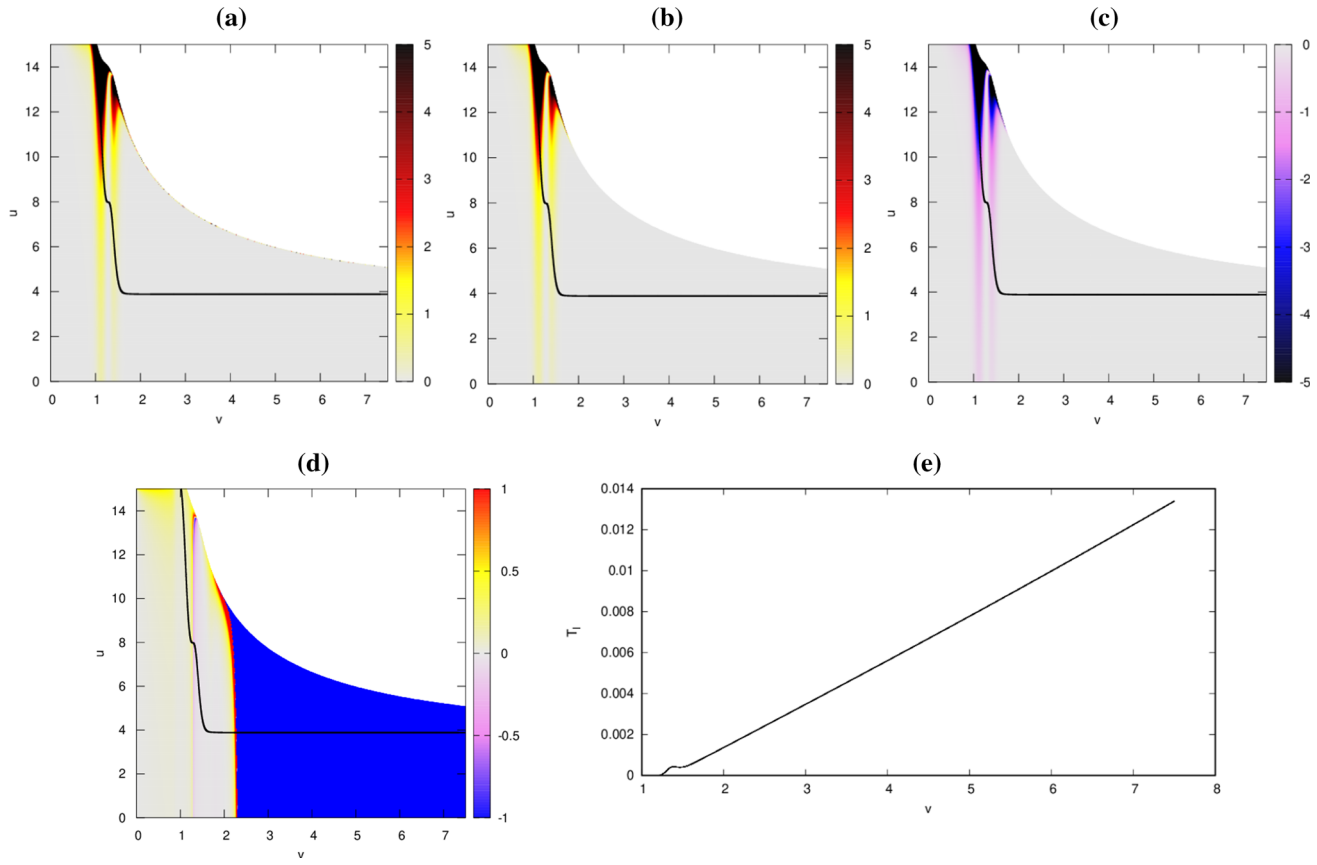

Fig. 15 The (vu)-distribution of **a** energy density, $\hat{\rho}$, **b** radial pressure, $\hat{p}_r$, **c** pressure anisotropy, $\hat{p}_a$, **d** tangential to radial pressures ratio, $\frac{\hat{p}_t}{\hat{p}_r}$, and **e** local temperature along the black hole apparent horizon, T_l, as a function of advanced time for a dynamical evolution characterized by parameters $\alpha = 0$, $\gamma = -0.1$ and $\tilde{p}_s = \tilde{p}_h = 0.04$ (the same as in Fig. 5b)

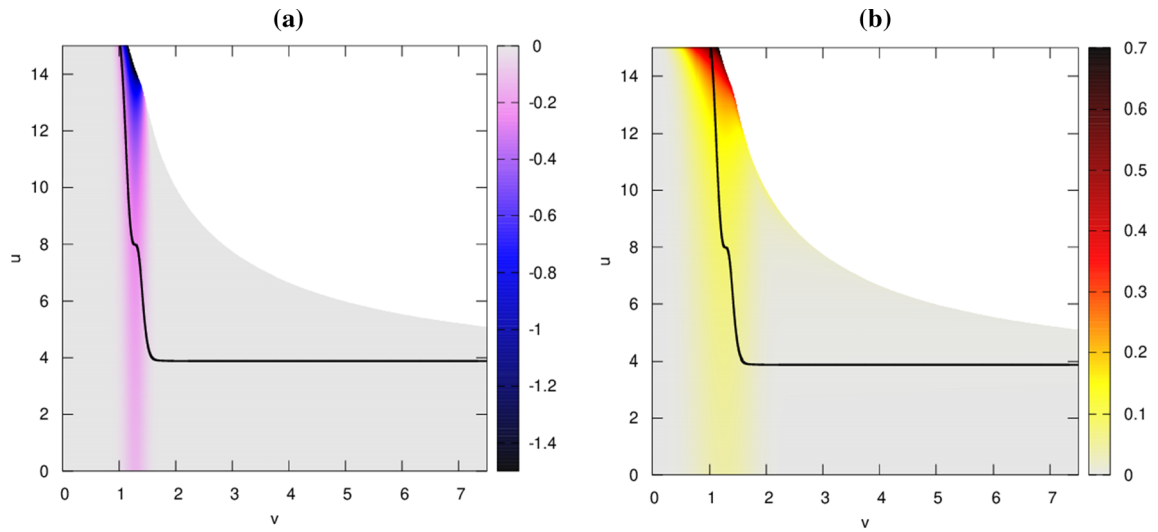

Fig. 16 The (vu)-distribution of **a** the neutral scalar field, h, and **b** the moduli of the complex scalar field, $|s|$, for the same parameters and field amplitudes as in Fig. 15

a conclusion that the Gauss–Bonnet term in the gravitational sector suppresses the tendency to form a Reissner–Nordström spacetime with an inner Cauchy horizon, whose appearance is characteristic for evolutions involving electric charge, can be drawn. The absolute value of the parameter γ influenced the v-range of the dynamical spacetime region, precisely the range of advanced time in which gravitational dynamics was observed was narrower for smaller values of $|\gamma|$.

The dependencies of the u-locations of the event horizons, radii and masses of black holes emerging from the investigated process on α and γ are qualitatively the same. As values of the model parameters increase, the black holes form later in terms of retarded time and both their radii and masses become smaller, up to an extremum, in which the tendencies reverse. Similar dependencies were observed in the case of non-minimal scalar–gravity couplings during dynamics investigations within the theory involving Higgs and dark matter sectors [27]. The only difference between the dependencies on the model parameters is that the changes are more significant for small values of α and large values of γ. The dependence of the values of black hole $U(1)$ charge on α and γ do not overlap the ones describe above. In the case of the dilatonic coupling constant, Q^{eh} increases significantly for its small values and decreases also significantly after reaching a maximum. In the case of the Gauss–Bonnet coupling, the black hole electric charge decreases monotonically within the whole parameter range.

The changes of the u-locations of the event horizons, radii, masses and electric charges of the nascent black holes with increasing self-interaction strengths of the evolving scalar fields are monotonic and qualitatively the same for various combinations of values of the model parameters α and γ. The features u^{eh} and Q^{eh} increase, while r^{eh} and m_H^{eh} decrease with the parameters. The changes are more significant for the electric charge in comparison to the remaining characteristics.

In all the investigated cases an increase of the energy density, radial pressure, pressure anisotropy and values of the collapsing scalar fields was observed along a null direction of propagation of the maxima of initially imposed field profiles in spacetime. For large absolute values of the γ parameter another increase in values of the quantities measured by an observer moving with the collapsing matter was visible in a close vicinity of the emerging singularity also for large values of advanced time. This implies a persisting non-trivial matter distribution around the central singularity. Additionally, an observation that the dilaton field possesses non-zero values outside the black hole event horizon may indicate a formation of a hairy black hole in this case. The local temperature calculated along the apparent horizon of the emerging black holes shows a late-time monotonic increase for all the investigated cases. Within dynamical spacetime regions, where inclinations of the horizons appear, the changes of the values of local temperature are not monotonic and extrema are observed.

The ultimate aim of the undertaken research is to investigate gravitational evolution of scalar fields in the full version of the EdGB theory in double null coordinates. These coordinates cover the whole spacetime, that is both the exterior and interior of objects that may arise in dynamically formed spacetimes. The presented analysis within the truncated version of the underlying theory is a first step towards calculations in the full EdGB. Its equations require a more sophisticated treatment, as they are coupled in a complicated way. The issue has been only partially resolved by introducing a shift symmetry in the case of coordinates, which do not penetrate emerging horizons, i.e., when only the exterior of the forming objects is possible to be thus dealt with [37].

Acknowledgements AN was supported by the National Science Centre, Poland, under a postdoctoral scholarship DEC-2016/20/S/ST2/00368. LN was supported by the National Science Centre, Poland, under a Grant DEC-2017/26/D/ST2/00193.

Data Availability Statement This manuscript has no associated data or the data will not be deposited. [Authors' comment: The datasets generated via numerical calculations and analysed during the current study are available from the corresponding author on reasonable request.]

Funded by SCOAP[3].

Appendix A: Numerical computations

Algorithm setup

The evolution of the studied physical system is described by Eqs. (2.29)–(2.45). It was resolved numerically. The set of equations of motion involves quantities d, q_1, q_2, y, s_1, s_2, h, a, p_1, p_2, x, r, f, g, Q, β. Each function depends on two null coordinates, namely advanced and retarded times. The dynamics of d, q_1, q_2 and y was followed along u in line with the equations $E4$, $S_{(Re)}$, $S_{(Im)}$ and D, respectively. The remaining quantities, s_1, s_2, h, a, p_1, p_2, x, r, f, g, Q and β, evolved along v according to the respective equations $P6$, $P7$, $P2$, $S_{(Re)}$, $S_{(Im)}$, D, $P4$, $E3$, $E2$, $M2$ and $M1$.

The system of evolution equations was solved in a bounded region of the (vu)-plane presented in Fig. 1 in Sect. 3. An

arbitrary null hypersurface of constant retarded time was taken as an initial data surface. The boundary conditions were posed on a hypersurface of constant advanced time. The two surfaces were marked as $u = 0$ and $v = 0$, respectively, for computational purposes.

Initial conditions are arbitrary profiles of the fields functions, s_1, s_2 and h, which were posed according to (3.2) and (3.1). The initial values along v of q_1, q_2 and y were calculated analytically using the relations $P6$ and $P7$. In the employed setup the distribution of matter is shell–shaped, hence the boundary is unaffected by it and the field functions s_1, s_2 and h vanish there. The boundary values of q_1, q_2 and y were obtained through integration of equations $S_{(Re)}$, $S_{(Im)}$ and D, respectively.

A gauge freedom to choose initial and boundary profiles of the r function remains within the investigated setup. $r\,(0, 0)$ was chosen to be equal to 7.5 for computational purposes. Initial and boundary values of g and f, respectively, determine the distances between the null lines and were chosen to be constant, that is $g\,(0, v) = \frac{1}{2}$ and $f\,(v, 0) = -\frac{1}{2}$. These values are justified by the fact that mass (3.4) should vanish at the central point $(0, 0)$. The r values on the initial null segment were obtained using the relation $P4$ and along the boundary with the equation $P3$. Initial and boundary profiles of f and g, respectively, were obtained via an integration of $E3$.

Initial values of the quantity d were calculated with the use of the equation $E2$, and its boundary values were obtained using $E4$. The spherical shell shape of the matter distribution justifies imposing the following boundary values: $a\,(u, 0) = 1$, $Q\,(u, 0) = \beta\,(u, 0) = 0$ and $p_1\,(u, 0) = p_2\,(u, 0) = x\,(u, 0) = 0$. Initial profiles of these functions were obtained using the equations $P2$, $M2$, $M1$, $S_{(Re)}$, $S_{(Im)}$ and D, respectively.

Employed schemes

The numerical code was written in Fortran from scratch. Integration along the u-coordinate involved the 2^{nd} order accurate Runge–Kutta method. Integration of the partial differential equations along advanced time was performed with the 2^{nd} order accurate Adams–Bashforth–Moulton method, except the first point, where the trapezoidal rule was used.

The double null coordinates selected for the analysis ensure regular behaviour of all the evolving quantities within the computational domain. Numerical difficulties arise as the event horizon is approached, as the function f diverges there. For this reason, a relatively dense numerical grid is indispensable to determine the horizon location and to examine the behaviour of fields beyond it, especially for large v-coordinate values. The efficiency of calculations was ensured by the use of an adaptive grid and performing integration with a smaller step in problematic regions. For the gravitational collapse investigations, a sufficient refinement algorithm is the one making the grid denser solely in the direction of retarded time [13]. The determination of the area of the computational grid, where it should be denser was made through a local error indicator. The quantity should be bounded with the evolving quantities and change its value significantly in adequate regions. The quantity $\frac{\Delta r}{r}$ along the u-coordinate meets the requirements and indicates the numerically problematic surrounding of the event horizon in spacetime [6].

Tests of the code

Analytical solutions do not exist for the investigated process and hence the accuracy of the code has to be checked via numerical possibilities in this regard. The convergence tests were performed for two evolutions characterized by the following parameters. Evolution 1 was initiated with $\alpha = -\sqrt{3}$, $\gamma = -0.01$, while Evolution 2 with $\alpha = -1$, $\gamma = -1$, and in both cases $\tilde{p}_s = \tilde{p}_h = 0.04$. The corresponding spacetime structures are presented in Figs. 2b and 3b, respectively.

To monitor the numerical outcomes convergence, the computations for Evolutions 1 and 2 were carried out on four grids with integration steps equal to multiples of $\delta = 10^{-4}$. An integration step of a particular grid was twice the size of a denser one. The convergence was examined on a hypersurface of constant retarded time selected arbitrarily with $u = 1$. The chosen hypersurface was located close to the forming event horizon in the region where the adaptive mesh on neither of the grids was active, what enabled a proper comparison of the results.

The evolving field functions along the chosen hypersurface of $u = const$ from within the range of advanced time in which the functions are initially non-vanishing for all the examined integration steps are shown in Fig. 17. The maximal observed discrepancy between the functions calculated on the grids with the smallest and biggest steps was equal to $2.55 \cdot 10^{-4}\%$. Figure 18 confirms the 2^{nd} order convergence of the numerical code. The maximal divergence between the field profiles obtained on two grids with a quotient of integration steps equal to 2 and their respective quadruples was $4 \cdot 10^{-1}\%$. The errors decreased as the grid density increased. The overall analysis revealed that the expected convergence was achieved and both the algorithm and the numerical code were appropriate for solving the obtained system of Eqs. (2.29)–(2.45) describing the dynamics of interest.

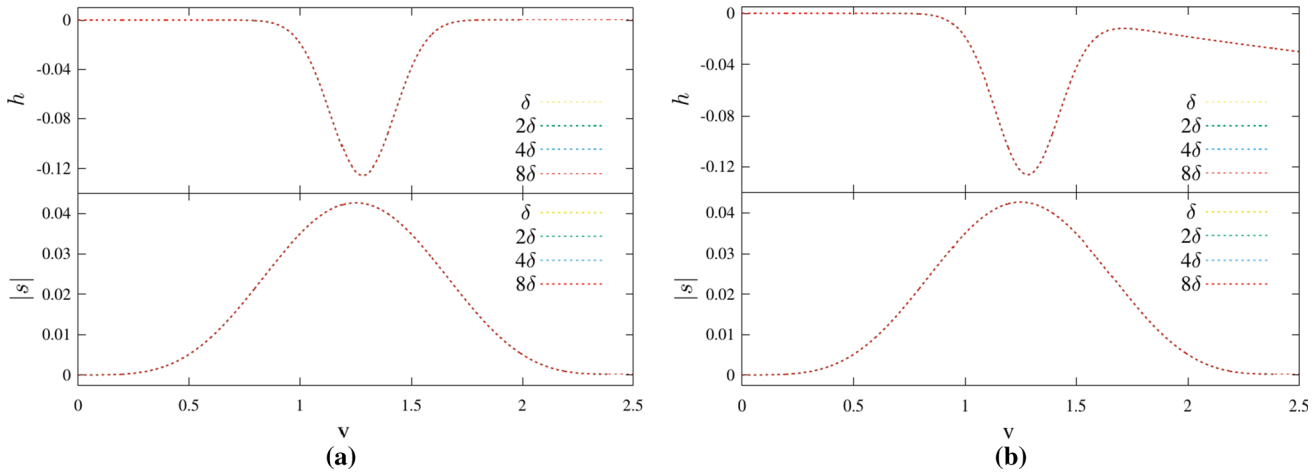

Fig. 17 The convergence of field functions. The scalar field, h, and the moduli of complex scalar field, $|s|$, were plotted versus v for evolutions conducted with integration steps, which were multiples of $\delta = 10^{-4}$, along hypersurfaces of constant u equal to 1 for **a** Evolution 1 and **b** Evolution 2

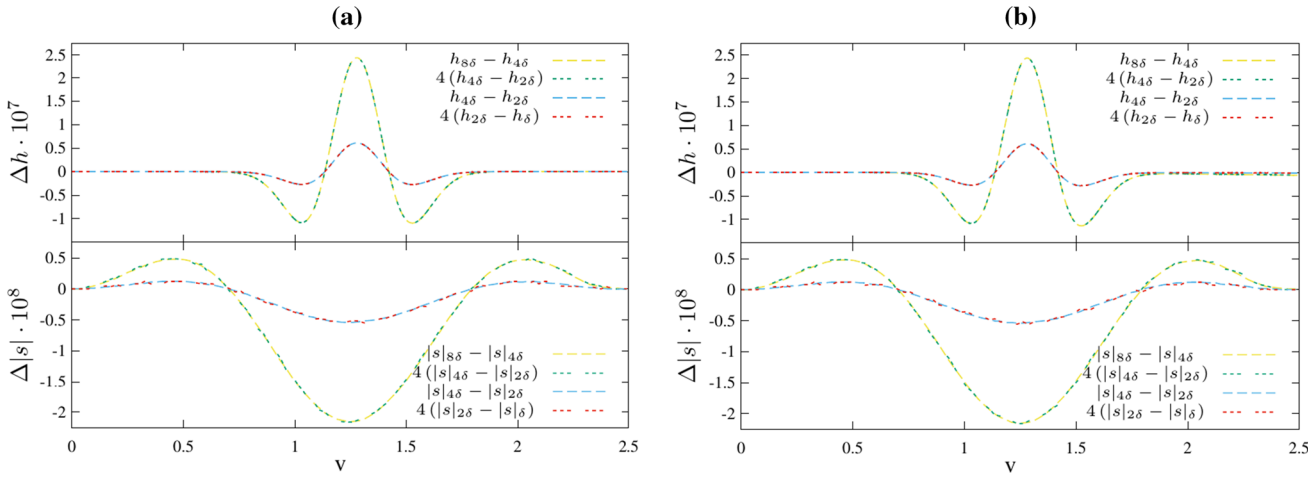

Fig. 18 The convergence of the code. The differences between the scalar field functions, Δh, and the moduli of complex scalar field, $\Delta|s|$, calculated on grids with different integration steps (multiples of $\delta = 10^{-4}$) and their multiples were obtained along the same hypersurfaces of constant u as in Fig. 17 for **a** Evolution 1 and **b** Evolution 2

References

1. E. Sorkin, T. Piran, The effects of pair creation on charged gravitational collapse. Phys. Rev. D **63**, 084006 (2001)
2. E. Sorkin, T. Piran, Formation and evaporation of charged black holes. Phys. Rev. D **63**, 124024 (2001)
3. R.S. Hamadé, J.M. Stewart, The spherically symmetric collapse of a massless scalar field. Class. Quantum Gravity **13**, 497 (1996)
4. S. Hod, T. Piran, Mass inflation in dynamical gravitational collapse of a charged scalar field. Phys. Rev. Lett. **81**, 1554 (1998)
5. S. Hod, T. Piran, The inner structure of black holes. Gen. Relativ. Gravit. **30**, 1555 (1998)
6. Y. Oren, T. Piran, Collapse of charged scalar fields. Phys. Rev. D **68**, 044013 (2003)
7. S.E. Hong, D. Hwang, E.D. Stewart, D. Yeom, The causal structure of dynamical charged black holes. Class. Quantum Gravity **27**, 045014 (2010)
8. D. Hwang, D. Yeom, Internal structure of charged black holes. Phys. Rev. D **84**, 064020 (2011)
9. J. Hansen, H. Dong-il, D.-H. Yeom, Dynamics of false vacuum bubbles: beyond the thin shell approximation. JHEP **11**, 016 (2009)
10. D. Hwang, D. Yeom, Responses of the Brans–Dicke field due to gravitational collapses. Class. Quantum Gravity **27**, 205002 (2010)
11. D.-I. Hwang, D.-H. Yeom, Generation of a bubble universe using a negative energy bath. Class. Quantum Gravity **28**, 155003 (2011)
12. D. Hwang, B. Lee, D. Yeom, Mass inflation in f(R) gravity: a conjecture on the resolution of the mass inflation singularity. JCAP **1112**, 006 (2011)
13. A. Borkowska, M. Rogatko, R. Moderski, Collapse of charged scalar field in dilaton gravity. Phys. Rev. D **83**, 084007 (2011)
14. A. Nakonieczna, M. Rogatko, Dilatons and the dynamical collapse of charged scalar field. Gen. Relativ. Gravit. **44**, 3175 (2012)
15. A. Nakonieczna, M. Rogatko, R. Moderski, Dynamical collapse of charged scalar field in phantom gravity. Phys. Rev. D **86**, 044043 (2012)

16. A. Nakonieczna, M. Rogatko, Phantom collapse of electrically charged scalar field in dilaton gravity. AIP Conf. Proc. **1514**, 43 (2013)
17. J. Hansen, D. Yeom, Charged black holes in string-inspired gravity: I. Causal structures and responses of the Brans–Dicke field. JHEP **10**, 040 (2014)
18. P. Chen, D.-H. Yeom, Cusp singularities in f(R) gravity: pros and cons. JCAP **10**, 022 (2015)
19. J. Hansen, D. Yeom, Charged black holes in string-inspired gravity: II. Mass inflation and dependence on parameters and potentials. JCAP **09**, 019 (2015)
20. A. Nakonieczna, M. Rogatko, Ł Nakonieczny, Dark sector impact on gravitational collapse of an electrically charged scalar field. JHEP **11**, 012 (2015)
21. D. Hwang, H. Kim, D. Yeom, Dynamical formation and evolution of (2+1)-dimensional charged black holes. Class. Quantum Gravity **298**, 055003 (2012)
22. D.-I. Hwang, B.-H. Lee, W. Lee, D.-H. Yeom, Bubble collision with gravitation. JCAP **07**, 003 (2012)
23. D.-I. Hwang, B.-H. Lee, C. Park, D.-H. Yeom, Inside and outside stories of black-branes in anti de Sitter space. Class. Quantum Gravity **30**, 235022 (2013)
24. A. Nakonieczna, J. Lewandowski, Scalar field as a time variable during gravitational evolution. Phys. Rev. D **92**, 064031 (2015)
25. A. Nakonieczna, D.-H. Yeom, Scalar field as an intrinsic time measure in coupled dynamical matter-geometry systems. I. Neutral gravitational collapse. JHEP **02**, 049 (2016)
26. A. Nakonieczna, D.-H. Yeom, Scalar field as an intrinsic time measure in coupled dynamical matter-geometry systems. II. Electrically charged gravitational collapse. JHEP **05**, 155 (2016)
27. A. Nakonieczna, Ł Nakonieczny, Gravitational dynamics in the toy model of the Higgs-dark matter sector: the field theoretic perspective. EPJC **80**, 1051 (2020)
28. A. Nakonieczna, Ł Nakonieczny, D.-H. Yeom, Black hole factory: a review of double-null formalism. Int. J. Mod. Phys. D **28**, 1930006 (2019)
29. I. Quiros, Selected topics in scalar-tensor theories and beyond. Int. J. Mod. Phys. D **28**, 1930012 (2019)
30. T. Kobayashi, Horndeski theory and beyond: a review. Rep. Prog. Phys. **82**, 086901 (2019)
31. A.R. Akbarieh, S. Kazempour, L. Shao, Cosmological perturbations in Gauss–Bonnet quasi-dilaton massive gravity. Phys. Rev. D **103**, 123518 (2021)
32. M.A. Cuyubamba, R.A. Konoplya, A. Zhidenko, No stable wormholes in Einstein-dilaton-Gauss–Bonnet theory. Phys. Rev. D **98**, 044040 (2018)
33. G. Tumurtushaa, D.-H. Yeom, Quantum creation of traversable wormholes ex nihilo in Gauss–Bonnet-dilaton gravity. EPJC **79**, 488 (2019)
34. H. Witek, L. Gualtieri, P. Pani, T.P. Sotiriou, Black holes and binary mergers in scalar Gauss–Bonnet gravity: scalar field dynamics. Phys. Rev. D **99**, 064035 (2019)
35. G. Tumurtushaa, D.-H. Yeom, Euclidean wormholes in Gauss–Bonnet-dilaton gravity (2020). arXiv:2006.04344
36. K. Yagi, L.C. Stein, N. Yunes, Challenging the presence of scalar charge and dipolar radiation in binary pulsars. Phys. Rev. D **93**, 024010 (2016)
37. J.L. Ripley, F. Pretorius, Gravitational collapse in Einstein dilaton-Gauss–Bonnet gravity. Class. Quantum Gravity **36**, 134001 (2019)
38. B. Robert, T.P. Sotiriou, H. Witek, Dynamical scalar hair formation around a Schwarzschild black hole. Phys. Rev. D **94**, 121503(R) (2016)
39. B. Robert, T.P. Sotiriou, H. Witek, Black hole hair formation in shift-symmetric generalised scalar-tensor gravity. Class. Quantum Gravity **34**, 064001 (2017)
40. J.L. Blázquez-Salcedo, F.S. Khoo, J. Kunz, Quasinormal modes of Einstein–Gauss-Bonnet-dilaton black holes. Phys. Rev. D **96**, 064008 (2017)
41. T. Ortín, *Gravity and strings* (Cambridge University Press, Cambridge, 2004)
42. C.W. Misner, K.S. Thorne, J.A. Wheeler, *Gravitation* (W. H. Freeman and Company, New York, 1973)
43. R.A. d'Inverno, J. Smallwood, Covariant 2+2 formulation of the initial-value problem in general relativity. Phys. Rev. D **225**, 1223 (1980)
44. S. Ayal, T. Piran, Spherical collapse of a massless scalar field with semiclassical corrections. Phys. Rev. D **56**, 4768 (1997)
45. M.W. Choptuik, Universality and scaling in gravitational collapse of a massless scalar field. Phys. Rev. Lett. **70**, 9 (1993)
46. S.W. Hawking, Gravitational radiation in an expanding universe. J. Math. Phys. **9**, 598 (1968)
47. A.B. Nielsen, M. Visser, Production and decay of evolving horizons. Class. Quantum Gravity **23**, 4637 (2006)
48. A.B. Nielsen, J.H. Yoon, Dynamical surface gravity. Class. Quantum Gravity **25**, 085010 (2008)